

NONDESTRUCTIVE DAMAGE CHARACTERIZATION WITH
EXAMPLES OF THERMAL AGING, NEUTRON
DEGRADATION AND FATIGUE

GERD DOBMANN
IRIS ALTPETER
KLAUS SZIELASKO
MARKUS KOPP

*Institut für zerstörungsfreie Prüfverfahren IZFP Fraunhofer-Gesellschaft University, Saarbrücken,
Germany; e-mail: gerd.dobmann@izfp.fraunhofer.de*

Nondestructive Testing (NDT) in the engineering community is normally associated with the objective to detect, to classify and to size material non-conformities – for instance beginning with nonmetallic inclusions of a size of some ten μm in steel or Aluminum alloys up to so-called 'material defects' like macroscopic cracks of some mm size. This objective, however, is at the top of the list of activities concerning the number of applications in non-destructive material testing worldwide. Methodologies like UT (Ultrasonic Testing) and RT (Radiographic Testing) or MT (Magnetic Testing) are well introduced in a wide field of product and component examination standards. In the last 15 to 20 years, the NDT technology was also developed for characterizing materials, for instance in terms of microstructure parameters, i.e. lattice defects, like distributions and densities of dislocations, precipitates, micro-voids, in order to describe strengthening and/or softening in materials, mainly in metal alloys, but also to measure the applied and residual stresses (Dobmann *et al.*, 1989).

Key words: NDT, damage characterization, micromagnetic techniques

1. Introduction

Starting in 1980, the first empirical approaches were developed, to characterize materials in terms of mechanically and technologically defined parameters such like hardness, hardness depth, yield limit and ultimate strength (Dobmann *et al.*, 1998), all of them standardized by a destructive procedure. In Borsutzki

(1998) it was published that these parameters could be determined also on-line in the steel making process, i.e. in a hot-dip galvanizing line for car body steel sheet production.

In this context, micromagnetic testing is especially suitable because micromagnetic parameters obtained under magnetic load show many similarities to mechanical parameters derived under mechanical loads. This is why microstructure parameters (lattice defects) impede dislocation movement as well as Bloch wall movement and relationships between mechanical and micromagnetic parameters are empirically derived by multiple parameter correlation, neural network and pattern recognition procedures (Altpeter *et al.*, 2002).

First publications to characterize the materials damage in terms of microscopic damage parameters such as creep damage porosity and fatigue effects were published in Dobmann *et al.* (1993), Dobmann and Seibold (1992). In the meantime further research work was initiated (Dobmann, 2002; Dobmann *et al.*, 2001a), some characteristic results of which are summarized in the following contribution. They mainly document the maturity of micromagnetic properties to solve this inspection task.

Metallurgists are familiar with the phenomenon of precipitation hardening which is usually associated with the elements carbon and nitrogen, the solubility of which is high in solid media, and which precipitate under heat treatment or specific service conditions as carbides or carbo-nitrides. Their contribution to the overall strength resides in the range of 10 to 12%, where the strengthening effect occurs due to an impeded dislocation movement under mechanical loading. Mikheev and Gorkunov (1979) have published abilities of micromagnetic parameters to characterize the strengthening effect of precipitation hardening.

In iron alloys, copper behaves in a similar way, so that in combination with neutron irradiation, even small contents of Cu can act as a driving force for embrittlement. These conditions, for instance, are present in our western nuclear pressure vessel steels where the copper content ranges from 0.01 to 0.07 wt%.

In case of the German martensitic/bainitic structural steel WB 36 (15NiCuMoNb5, 1.6368) which is in service in fossil power plants but also in pipes and pressurizers of German nuclear power plants, the effects of precipitation hardening are much larger. WB 36 has an average composition with C – 0.15, Ni – 1.15, Cu – 0.65, Mo – 0.35 and Nb – 0.025 (all amounts in wt%).

The 2nd chapter of this contribution will present the results obtained at different heats of WB 36 steel and will introduce it in the applied 3MA-NDT-technology.

In the 3rd chapter, the results obtained in GRETE (1999) and documenting the sensitivity of NDT-technology to characterize neutron degradation in pressure vessel materials are presented. However, in Germany the radiation conditions concerning nuclear pressure vessels are different compared with other countries and therefore the micromagnetic technology has to be validated in an ongoing project.

The 4th chapter of the contribution is devoted to the characterization of fatigue damage. In the low cycle as well as in the high cycle regime, austenitic and ferritic steel specimens were fatigued. A new NDT technique based on measurement of the transfer-impedance of an eddy current yoke transducer in combination with a Giant Magnetic Resistor (GMR) gradiometer (Grünberg, 1995) was applied to on-line monitoring of the fatiguing process.

2. ND-characterization of thermal aging of WB 36 steel

2.1. The material

In the typical "as delivered" state of WB 36, half of the contained Cu is already precipitated, while the other half remains in solid solution. After long term service exposure above 320°C, damage was observed due to further precipitation of Cu; an increase in yield strength $\Delta\sigma_y = \pm 150$ MPa and a shift of the fracture appearance transition temperature $\Delta_{FATT} = +70^\circ\text{C}$ can be measured. Small angle neutron scattering revealed the fact that the mechanical property changes were caused by Cu precipitates ranging from 1 to 1.5 nm in size. The particles are coherent from the bcc structure and therefore arose a high level of compressive residual stress in their vicinity, balanced by tensile stresses in the environmental matrix. The precipitation hardening can be characterized by Vickers hardness measurements in the laboratory; the effect is in the range of 40 HV 10 units. At a component in service, however, hardness measurements cannot be applied in an area-wide manner, which creates a demand for the development of a suitable NDT technique.

Magnetic and, in particular, micro-magnetic techniques are suitable for the characterization of mechanical property changes. This relates to the fact that microstructure and lattice defects which impede the movement of dislocations and therefore contribute to the mechanical strengthening, impede the movement of Bloch walls in magnetizable materials in a similar way. This can be documented in micro-magnetic properties such as coercivity, Barkhausen noise, non-linearity, etc. Fraunhofer IZFP applies the so-called 3MA approach

(Altpeter *et al.*, 2002) which combines several independent micro-magnetic properties in a regression or similar data fusion model, in order to predict the mechanical property changes at a component. This contribution discusses the results obtained with the 3MA approach in case of the steel WB 36.

On a set of approximately 70 round samples (80 mm in length, diameter 6 mm) of the steel grade WB 36, thermal service exposure was simulated in an accelerated manner through long-term annealing at 400°C. The two examined heats E2 and E59 represent admissible variants of WB 36, where E2 originates from a hot-rolled plate and E59 from a pressure vessel drum.

The samples of the heat E59 were in service-exposed condition (57000 h at 350°C) and had to be recovery-annealed (3 h at 600°C) prior to service simulation. Half of the recovery-annealed samples underwent a stabilizing heat treatment at the Materials Testing Institute (MPA) at the University of Stuttgart which also performed the subsequent service simulation and parts of the materials characterization.

Although the samples of the heat E2 were not service-exposed in the beginning, 13 samples were recovery-annealed (3 h at 600°C) in order to relieve possible surface stresses and characterize their influence on the measured results. In addition, 8 samples were plastically deformed to specific amounts (5%, 11% in longitudinal direction) for the simulation of practical disturbances. The service simulation and mechanical characterization of the E2 material took place at IZFP.

All heat-treatments were done using an electric furnace with internal air circulation. Samples of each initial condition were removed from the furnace piece by piece in short time intervals in order to obtain a fixed set of differently aged material. All electro-magnetic tests were performed on this sample set. Additionally, the Vickers hardness (HV 5) was recorded with a 95% confidence interval of less than ± 5 HV 5 by using a Krautkrämer TIV hardness tester. Fig. 1 shows the obtained Vickers hardness values and the residual electrical resistance quotient (G – a measure for the amount of precipitated copper, obtained by MPA) for the heat E2. The maximal increase in hardness versus the initial material state was observed to be around 25 HV 5 in any case, and it was reached after 600 to 1000 hours of service simulation. Due to a higher dislocation density, plastically deformed samples exhibit higher initial hardness and quicker ageing. Fig. 2 shows the corresponding data for the heat E59, which has a higher initial hardness and slower ageing as compared to the heat E2. The maximum hardness of E59 will probably be reached beyond 15 000 h of service simulation.

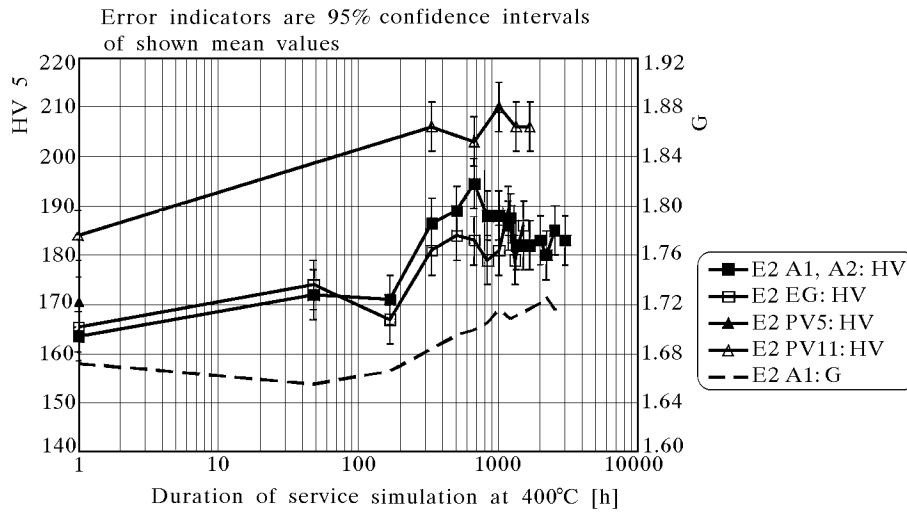


Fig. 1. Vickers hardness (HV 5) and quotient of residual electrical resistance (G) as a function of service simulation time for the heat E2. Initially, the subsets A1 and A2 were as delivered, EG was recovery-annealed, and PV5/PV11 were plastically deformed by 5% and 11%, respectively

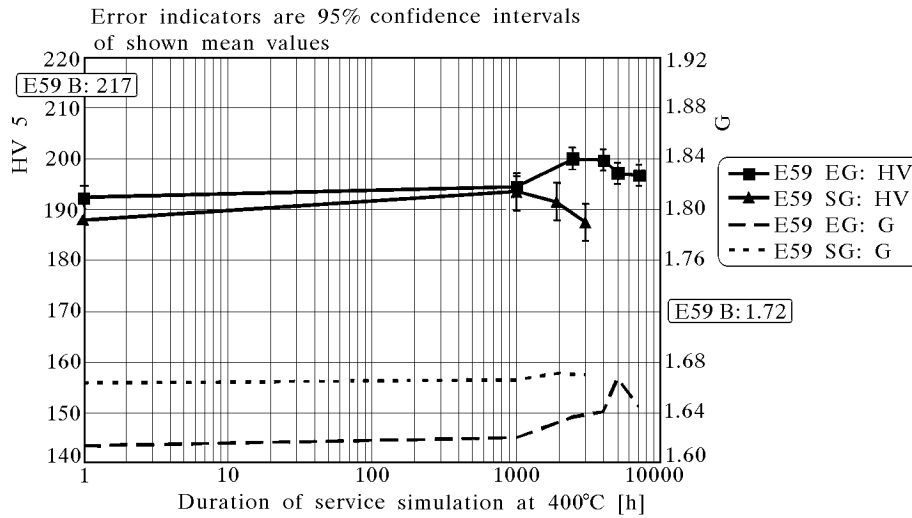


Fig. 2. Vickers hardness (HV 5) and coefficient of residual electrical resistance (G) as a function of the service simulation time for the heat E59. The subset EG was recovery-annealed from the service-exposed state B. The heat-treatment stabilized subset is denoted by SG

2.2. The experiments

A U-shaped electromagnet was used to excite an alternating magnetic field along the longitudinal axis of the sample. A disc-shaped pickup coil and a temperature-stabilized hall probe were used to record Barkhausen noise events and magnetic field strength, respectively. The Barkhausen noise signal was amplified by 60 dB and bandpass-filtered to a range of 5-200 kHz. All signals were digitized using common data acquisition hardware. The Barkhausen noise signal was then digitally re-filtered for separate analysis of its different frequency components. Characteristic scalar quantities (Altpeter, 1990) were extracted from the envelope of the Barkhausen noise signal as a function of the applied magnetic field strength. Moreover, an upper harmonics analysis (Pitsch, 1989) of the magnetic field strength signal was performed and characteristic quantities were derived. As changes in conductivity may be expected due to copper precipitation, a simplified eddy current analysis procedure was performed based on the relationship between magnetic field strength and exciting voltage of the electromagnetic coil. The scalar result quantities of all three methods (Barkhausen noise, upper harmonics and eddy current analysis) are combined to a vector which characterizes the material condition.

The total set of samples was split up into a large training set and a small test set. Using the above-mentioned electromagnetic methods, calibration data were recorded for the training set and assigned the corresponding Vickers hardness values. For the replication of practical circumstances, an additional tensile load of 5 to 100 MPa was applied to the sample in its longitudinal direction (a minimum load was required in order to prevent vibrations due to the alternating magnetic field). The amount of tensile load was varied both during calibration and the test, but remained unknown to the system, so as to constitute a realistic disturbing factor. The 3MA approach which is pursued at IZFP solves the inverse problem of target quantity prediction from a limited set of calibration data (Dobmann and Höller, 1990). In this case, a specialized pattern recognition algorithm (Tschuncky, 2004) based on a nearest neighbour search was used to obtain approximate values of the Vickers hardness during the repeated measurement on both the calibration set and the test set.

Fig. 3 shows the obtained results in case of no external loading. The RMS error (RMSE, residual standard deviation) of the predicted values is around 2 HV 5, corresponding to a 95% confidence interval of ± 4 HV 5. The prediction error within the calibration set falls short of the reference confidence (± 5 HV 5), which shows that the samples differ significantly from each

other in terms of their electromagnetic properties. This enables the accomplishment of additional disturbances like-superimposed tensile loads, as shown in Fig. 4. The RMS error drops to around 4 HV 5 in this case (equivalent to a 95% confidence interval of ± 8 HV 5), which is still within the expected frame of accuracy, considering the disturbing influence of varying tensile load.

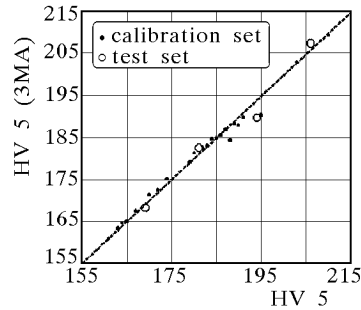


Fig. 3. Predicted Vickers hardness for WB 36, heat E2, subsets A1, A2, EG, PV5 and PV11 versus actual Vickers hardness. Averaged statistics: $R^2 \approx 0.98$, RMSE ≈ 2 HV 5

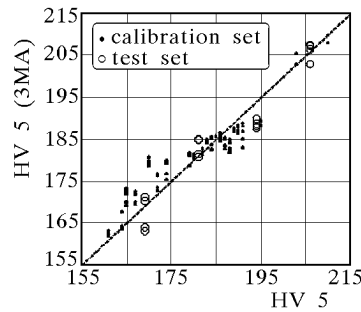


Fig. 4. Same as above, but with superimposed tensile load from 5 to 100 MPa during both calibration and test. Averaged statistics: $R^2 \approx 0.91$, RMSE ≈ 4 HV 5

In addition to the Vickers hardness, the 3MA approach predicted the quotient of residual electrical resistance (G) or the equivalent service simulation time with similar accuracy. These findings were also confirmed in case of the heat E59. However, as there has not been much change in hardness to date, an in-depth evaluation must follow as soon as the corresponding service-simulation is finished.

3. ND-characterization of neutron degradation

Depending on the specific design – which is different in different countries of the world – the pressure vessel material in nuclear power plants is exposed to a neutron flux which is in the range between $5 \cdot 10^{18}$ n/cm² (German design) in 32 years at 288°C, and $8 \cdot 10^{19}$ n/cm² at 254°C in 14 years (French experience). The energy input of the neutrons is directly producing lattice defects like vacancies and indirectly by stimulating the precipitation of Cu-rich precipitates. These are in the 3nm diameter range and coherent in the bcc lattice, and can be detected by small angle neutron scattering. Both the vacancies and the precipitates reduce the toughness of the material, which can be characterized by a reduction of the Charpy energy and a shift in the fracture appearance transition temperature to higher temperatures.

In practice the material degradation is characterized in surveillance programmes by using a standardized Charpy V-notch specimen and the tensile test specimen made of the pressure vessel material and its weldments. The specimens are exposed in special radiation chambers near the NPP core at a higher fluence than that at the surface of the pressure vessel wall. These specimens from time to time are removed from the chambers and used for destructive tests in order to document the state of microstructure change.

Under the headline of lifetime extension of the NPPs, longer than the ~ 30 years initially prospected, there will be not enough material available and therefore nondestructive tests should replace the destructive ones. Furthermore, to assure and to document a higher nuclear safety between two subsequent destructive tests, one would like to have many nondestructive tests and the ND-technology should also be developed to an in-service inspection method to be applied at the pressure vessel inner surface.

That was the reason to investigate, in an inspection trial of the European research programme EURATOM the ability of different ND-techniques to characterize the material degradation due to neutron irradiation. Different materials from surveillance programmes of different European countries were investigated by different teams in the hot cell of the research power plant in Petten, Netherlands. Table 1 gives an overview about the materials and the exposure conditions. There were two sets of specimens of France of the power plants Chinon and Dampierre and two sets coming from Germany (research centre Rossendorf), a reference heat JRQ according to the Japanese standards and an optimized heat concerning the Cu-content, called JFL. In addition, SKODA from the Czech Republic has supplied with a set of specimens according to the Russian design. Table 2 is documenting the experimental

data. Whereas for the first four sets of specimens the transition temperature T09 is documented, the SKODA specimen are characterized by the transition temperature of the Charpy energy at 41 joule.

Table 1. Irradiation conditions and destructively determined mechanical properties

Supplier	Heat	Cu-content [%]	Fluence in 1 MeV 10^{19} n/cm ²	Irradiation temp. [°C]	Transition temp. T09 [°C]
France	Chinon B1	0.07	0		-32.0
			1.74	300	-10.0
			3.03	300	7.0
			4.65	300	13.0
			6.64	300	21.0
France	Dampierre M3	0.044	0		-26.0
			1.74	300	-10.0
			3.74	300	0
			5.36	300	20.0
			7.56	300	31.0
Germany	JRQ	0.14	0	254	-8.6
			0.72	254	103.4
			5.61	254	171.9
			9.58	254	240.4
Germany	JFL	0.01	0		-45.9
			0.62	254	-21.7
			4.41	254	15.8

Table 2. Heats according to the Russian design

Supplier SKODA WWER mat.	Fluence in 0.5 MeV 10^{19} n/cm ²	Irradiation temperature [°C]	Transition temperature T41 [°C]
3 specimen	0	fresh	-90
3 specimen	2.9	288	-72
3 specimen	9.7	288	-32

The German heat JRQ is the one with the highest Cu-content and therefore one can observe the greatest shift in the transition temperature. Generally the transition temperatures were calculated according to a th-curve fit from the Charpy energy data.

IZFP has applied 3MA-approaches (Altpeter *et al.*, 2002) to calibrate regression models. One part of each specimen set was used to calibrate and the other part – independently selected – was taken to test the model. Because of the fact that all of the specimens were only available as half-Charpy-specimens after performing the destructive test side-effects of residual stresses and plastic deformation were observed.

In Figure 5 the results of the regression calibration and the tests are documented according the specimens of Table 1. The correlation coefficient is 97.6 – very close to 100% and the residual standard deviation is 15.6°C (5.4%). However, by testing the calibration with the independent test specimens, a much larger standard error is obtained (54.1°C, 18.9%) The reason for this discrepancy was discussed before and it is the influence of the plastic deformation in these specimens.

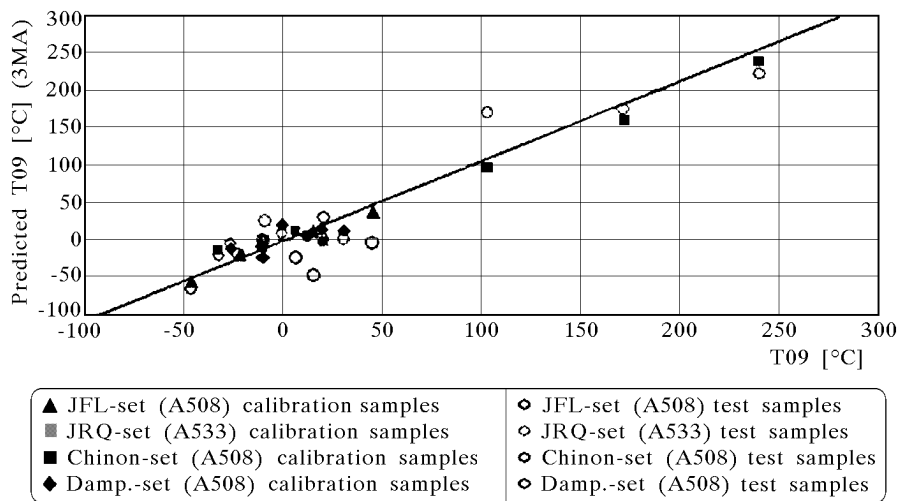


Fig. 5. The prediction of the T09-transition temperature by 3MA (correlation coefficient for calibration JFL, JRQ, Chinon, Dampierre together, $cc = 99.7$, standard error is equal 15.6 (5.4%) for calibration samples and 54.1 (18.9%) for test samples)

The same situation can be observed in Figure 6 when discussing the Russian heat delivered by SKODA. In that case the regression calibration can be performed and an excellent correlation coefficient of 99.7 is obtained with a standard error of 1.8°C (3.1%). Using the independently selected test specimens, however, the standard error of estimate is with 14.5°C (24.9%) much larger. In order to overcome the side effects of the plastic deformation in further investigations, the 3MA-approach has to be calibrated at unbroken Charpy specimens.

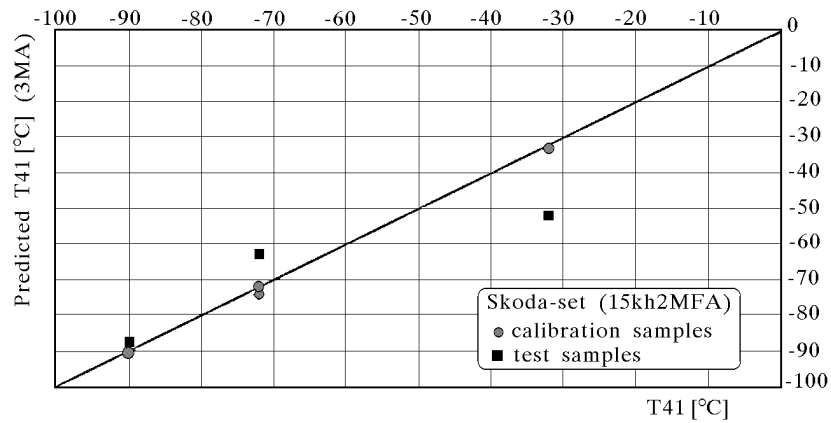


Fig. 6. The prediction of the T41-transition temperature at the Russian heat by 3MA (correlation coefficient $cc = 99.7$, standard error is equal 1.8 (3.1%) for calibration samples and 14.5 (24.9%) for test samples)

4. ND-characterization of fatigue

Austenitic stainless steels are in widespread application in the chemical as well as nuclear industry, mainly because of their high toughness and insensitivity against corrosion attack. However, under static as well as fatigue load, the material has the tendency to respond with localized phase transformations from the non-magnetic γ - to the martensitic and ferromagnetic α' -phase. The process starts localized at positions of higher stress intensity, i.e. at microstructure inhomogeneities like non-metallic inclusions and carbo-nitride precipitates.

The amount of martensite as well as its magnetic properties should provide information about the fatigue damage. Fatigue experiments were carried out at different stress and strain levels at Room Temperature (RT) and at $T = 300^\circ\text{C}$. The characterization methods included microscopic techniques such as light microscopy, REM, TEM and Scanning Acoustic Microscopy (SAM) as well as magnetic methods, ultrasonic absorption, X-ray and neutron diffraction (Bassler, 1999; Lang, 2000). As the martensitic volume fractions are especially low, for in-service temperatures of about 300°C highly sensitive measuring systems are necessary. Besides systems on the basis of HT_C-SQUID (Kittel, 1971) (High Temperature Super Conducting Quantum Interference Devices), special emphasis was on the use of GMR-sensors [19] (Giant Magneto Resistors), which have the strong advantage to be sensitive also for DC-magnetic fields without any need for cooling. In combination with an eddy-current transmitting coil and an universal eddy-current equipment,

as a receiver the GMR-sensors were used especially to on-line monitoring of the fatigue experiments in the servo- hydraulic fatigue machine.

Pure ferritic steels do not show phase transformation as a function of cyclic or quasi-static loading. Therefore the strong magnetic effect observed in the austenitic material by martensite formation is not detected. The plain carbon steel C15 (nominal 0.15% carbon) is a characteristic example for this case. The cyclic loading here only enhances the dislocation density (some orders of magnitude) and is influencing the development of characteristic dislocation networks and cell structures. The cyclic deformation behavior of this group of steels is well understood (Dobmann *et al.*, 2001b). In stress-controlled fatigue tests the measured plastic strain amplitude is a sensitive quantity to measure the changes in the dislocation network and cell structure, which are the reasons for the cyclic softening and cyclic hardening.

4.1. Materials

Table 3 documents the chemical composition of the steel 1.4541 and Table 4 for the plain carbon steel C15. In the case of the austenitic stainless steel two heats were investigated in order to see also the effect of different charges, i.e. manufacturer influences of nominally the same quality.

Table 3. Chemical composition of the stainless steel 1.4541 in mass [%]

Elements	C	N	Si	Mn	P	S	Cr	Mo	Ni	Ti
Heat 1	0.05	0.002	0.4	1.09	0.024	0.005	17.81	0.27	9.3	0.3
Heat 2	0.03	0.006	0.45	1.72	0.022	0.014	17.31	0.28	10.18	0.16

Table 4. Chemical composition of the plain carbon steel C15 in mass [%]

Elements										
C	Si	Mn	P	S	Cr	Ni	Mo	Cu	N	Al
0.15	0.189	0.43	0.0134	0.025	0.132	0.037	0.011	0.014	0.007	0.037

In any case the experiments were performed at specially designed (Bassler, 1999), "hourglass"-shaped fatigue specimens as shown in Figure 7.

4.2. NDT-techniques applied

Two types of magnetic sensors were utilized for characterizing the fatigue behavior, different SQUID-magnetometer (Kittel, 1971) and GMR [19]. For on-line measuring at the servo-hydraulic machine only the GMR sensors were

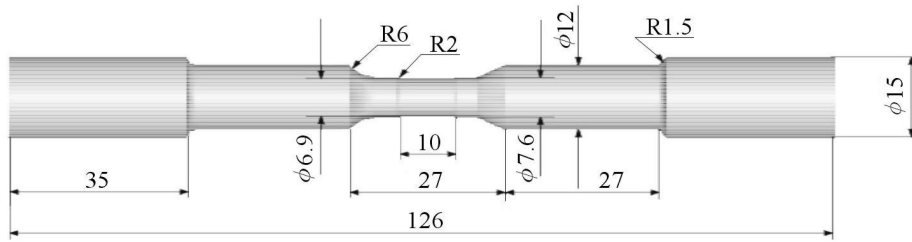


Fig. 7. Hourglass-shaped fatigue specimen used in the experiments

used. Figure 8 gives a view on the sensor together with the clip gage and the fatigue specimen in the machine. The GMR was controlled by standard eddy-current equipment and can be applied as magnetometer or can measure a transfer-impedance between a small electromagnetic yoke as transmitter coil and the GMR as a receiver. The measurement technique is described in detail in Lang (2000), Eifler and Macherauch (1990).

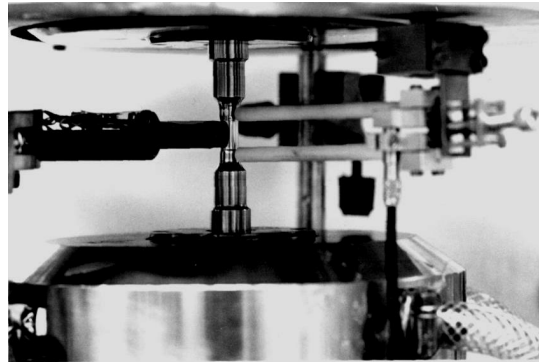


Fig. 8. GMR-sensor for on-line fatigue monitoring

4.3. Fatigue tests and on-line monitoring results

In the case of the steel 1.4541 the GMR-sensor was applied as magnetometer and as an eddy-current receiver. Because of the increasing content of the ferromagnetic martensitic phase in the austenitic matrix, a continuous enhancement of the magnetic field strength is observed. Performing the on-line monitoring experiment some more effects can be documented. Figure 9 presents the results for a strain-controlled LCF fatigue test ($\varepsilon_{a,p} = 0.2\%$, $R_\varepsilon = 1$, room temperature).

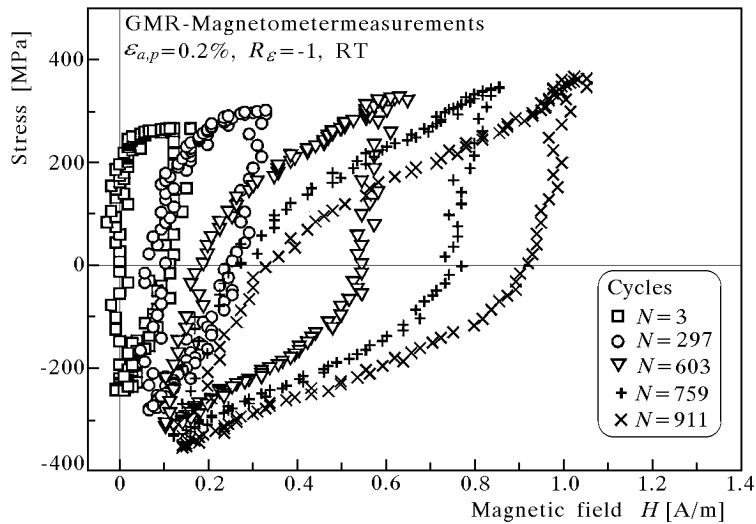


Fig. 9. Stress versus magnetic field hysteresis curves

In this case a change of the stress amplitude at the specimen with increasing load cycles is observed, i.e. a cyclic strengthening. Similar to a cyclic hysteresis curve, cyclic stress versus magnetic field hysteresis curves can be measured. For different distinct load cycles these curves are presented. With increasing load cycle number, the *area of the curves* is increasing as well as the central point, which can be defined as a "mean magnetic field value". Furthermore, a shearing of the curves is observed too.

In stress-controlled fatigue tests the eddy current transfer-impedance measured by the GMR-sensor was found to be especially suitable to characterize the fatigue behavior. Figure 10 is an example for a multiple step fatigue test with a load mix of different amplitudes and time dependences. The impedance ZGMR clearly shows in average a continuous increasing due to the martensite development (offset). However, this offset curve is modulated by a time function, which exactly follows the plastic strain amplitude. Cyclic softening and cyclic hardening are visualized.

The plain carbon steel C15 was fatigue-tested in single step stress-controlled HCF experiments. Also here the GMR-transfer-impedance was measured to characterize the fatigue behavior. Figure 11 documents the total strain amplitude $\varepsilon_{a,t}$ and the transfer-impedance Z_{GMR} as a function of the load cycles in a cyclic deformation curve. The ferritic steel shows cyclic softening followed by cyclic strengthening. The impedance as a function of the load cycles shows also an increase to a maximum followed by a decrease.

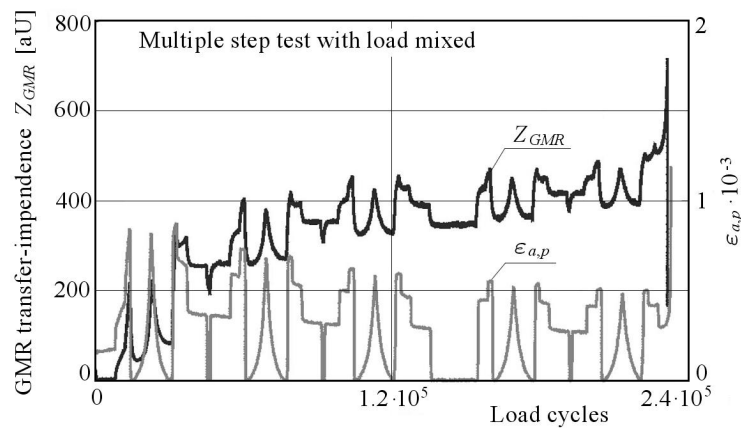


Fig. 10. GMR transfer-impedance and plastic strain amplitude for a multiple step load mix at the austenitic stainless steel 1.4541

However, here the dislocation multiplication, dislocation networking and cell sub-structures primarily influence the electrical conductivity and the magnetic permeability. A dislocation multiplication – mainly in the first phase of fatigue – reduces the electrical conductivity. Therefore the impedance is in this first phase less sensitive than the strain amplitude, and the maximum is reached also later, with a time delay compared with the strain. However, the secondary strengthening is clearly visualized and is due to the permeability effects and can be discussed as an influence of compressive residual stresses of higher order.

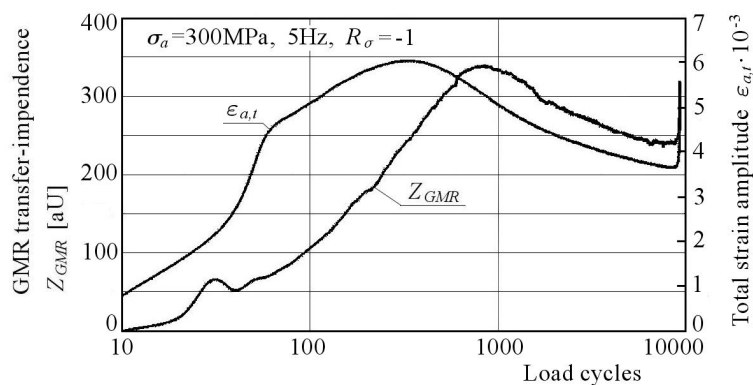


Fig. 11. Total strain amplitude and the GMR transfer-impedance at the plain carbon steel C15

5. Conclusion

- Micromagnetic techniques have a wide potential to characterize the materials damage.
- Precipitation hardening by thermal aging can be described by use of a micromagnetic multiple parameter approach on a high confidence level.
- Neutron degradation is a complex material damage and the micromagnetic approach needs further investigations when Charpy specimens should be used for calibration because of side-effects by plastic deformation and residual stresses in the broken specimens. Furthermore the sensitivity of the technology has to be validated for much lower fluences during lifetime.
- The ability by micromagnetic NDT to follow fatigue damage in the early stages, i.e. before surface cracking can be observed, and a special on-line monitoring technique was presented characterizing the cyclic softening and hardening effects.

References

1. ALTPETER I., 1990, *Spannungsmessung und Zementitgehaltsbestimmung in Eisenwerkstoffen mittels dynamischer magnetischer und magnetoelastischer Messgrößen*, PhD-Thesis, Saarland University (in German), Saarbrücken, Germany
2. ALTPETER I., BECKER R., DOBMANN G., KERN R., THEINER W., YASHAN A., 2002, Robust solutions of inverse problems in electromagnetic non-destructive evaluation, *Inverse Problems*, **18**, 1-15, Institute of Physics Publishing
3. BASSLER H.-J., 1999, *Wechselverformungsverhalten und verformungsinduzierte Martensitbildung bei dem austenitischen Stahl X6 CrNiTi 1810*, PhD-Thesis, University Kaiserslautern (in German)
4. BORSUTZKI M., 1998, *Process-Integrated Determination of the Yield Strength and Deep Drawability Parameters r_m und Δr at Cold-Rolled and Hot-Dip-Galvanized Steel Sheets*, Ph.D. Thesis, Saarland University (in German), Saarbrücken

5. DOBMANN G., 2002, On-line monitoring of fatigue in the LCF and HCF range by using micro-magnetic NDT at plain carbon and austenitic stainless steel, *8th ECNDT*, Barcelona, Spain, June 17-21, *Technical Area Material Characterization, Conference Proceedings*, Spanish Society for NDT
6. DOBMANN G., ET AL., 1989, Progress in the micromagnetic multiparameter microstructure and stress analysis (3MA), In: *Nondestructive Characterization of Materials, III*, P. Höller, V. Hauk, G. Dobmann, C. Ruud, R. Green (edit.), Springer-Verlag, Berlin, p. 516
7. DOBMANN G., ET AL., 1998, Barkhausen noise measurements and related measurements in ferromagnetic materials, In: *Topics on Nondestructive Evaluation Series*, B.B. Djordjevic, H. Dos Reis (edit.), Vol. 1: *Sensing for Materials Characterization, Processing, and Manufacturing*, G. Birnbaum, B. Auld (edit.), The American Society for Nondestructive Testing, Inc., ISBN 1-57117-067-7
8. DOBMANN G., DEBARBERIS L., COSTE J.-F., 2001, Aging material evaluation and studies by non-destructive techniques (AMES-NDT), a European network project, *Nuclear Engineering and Design*, **26**, 363-374
9. DOBMANN G., HÖLLER P., 1990, Non-destructive determination of material properties and stresses, *10th Int. Conf. NDE in the Nuclear and Pressure Vessels Industries*, Glasgow, ASM Int.
10. DOBMANN G., KRÖNING M., THEINER W., WILLEMS H., 1993, Non-destructive characterization of materials by ultrasonic and micro-magnetic techniques for strength and toughness prediction and the detection of early creep damage, *Staatliche Materialprüfungsanstalt –MPA*, Stuttgart: German-Japanese Joint Seminar on Structural Strength and NDE Problems, Nuclear Engineering. Sec. 3.4, Stuttgart
11. DOBMANN G., LANG M., EIFLER D., BASSLER H.-J., 2001, On-line fatigue monitoring of austenitic stainless steel using a GMR-sensor, In: *Studies in Applied Electromagnetics and Mechanics*, J. Pávo, G. Vértesy, T. Takagi, S.S. Udpa (edit.), Amsterdam, Washington, Tokyo: IOS Press, p. 342, *Proceedings of the International Workshop on Electromagnetic Non-Destructive Evaluation*, June 2000, Budapest, ISSN: 1383-7281
12. DOBMANN G., SEIBOLD A., 1992, First attempts towards the early detection of fatigued substructures using cyclic-loaded 20MnMoNi 55 steel, *Nuclear Engineering and Design*, **137**, 363-369
13. EIFLER D., MACHERAUCH E., 1990, Microstructure and cyclic deformation behaviour of plain carbon and low-alloyed-steels, *Int. Journal of Fatigue*, **12**, 3, 165-174
14. GRETE, 1999, Evaluation of NDT techniques for monitoring of material degradation, EURATOM programme, FIS5-1999-00280
15. GRÜNBERG P., 1995, Riesenmagnetowiderstand in magnetischen Schichtstrukturen, *Physikalische Blätter*, **51**, 1077-1081

16. KITTEL CH., 1971, *An Introduction to Solid State Physics*, J. Wiley and Sons, New York
17. LANG M., 2000, *Zerstörungsfreie Charakterisierung des Wechselverformungsverhaltens und der verformungsinduzierten Martensitbildung bei dem austenitischen Stahl X6 CrNiTi 1810 mittels empfindlicher Magnetfeldsensoren*, PhD-Thesis, Saarland University (in German), Saarbrücken
18. MIKHEEV M.N., GORKUNOV E.S., 1979, Magnetic methods of monitoring quality of heat treatment, *Ninth World Conference on Non-Destructive Testing*, **4A-10**, Melbourne
19. NVE Electronics, Magnetizable Bead Detector, United States Patent Application, 20020060565, 2002
20. PITSCH H., 1989, *Die Entwicklung und Erprobung der Oberwellenanalyse im Zeitsignal der magnetischen Tangentialfeldstärke als neues Modul des 3MA-Ansatzes (Mikromagnetische Multiparameter Mikrostruktur und Spannungsanalyse)*, PhD-Thesis, Saarland University (in German), Saarbrücken, Germany
21. TSCHUNCKY R., 2004, *Entwicklung eines Mustererkennungs- und Klassifikationsmoduls für die indirekte Charakterisierung von Werkstoffeigenschaften*, Diploma Thesis, Saarland University (in German), Germany

Nieniszcząca charakteryzacja uszkodzenia materiału w odniesieniu do termicznego starzenia, degradacji neutronowej i zmęczenia

Sreszczenie

Badania nieniszczące (NDT) są zwykle, w społeczności inżynierskiej, wiązane ze zdolnością do wykrycia, klasyfikacji i wymiarowania niezgodności materiałowych – na przykład z początkiem niemetalicznych wtrąceń o rozmiarach kilku dziesiątek mikrometra dla stali lub stopów aluminium, aż do tak zwanych „defektów materiałowych” w rodzaju pęknięć makroskopowych o rozmiarach kilku milimetrów. Cel ten jest jednak na szczycie listy podejmowanych działań w szeroko rozumianych nieniszczących badaniach materiałowych. Metodologie w rodzaju BU (badań ultradźwiękowych), BR (badań radiograficznych) czy BM (badań magnetycznych) są dobrze wprowadzone w szerokiej dziedzinie standardowych badań wyrobów i ich składników. W ostatnich 15-20 latach techniki nieniszczące rozwijano również w odniesieniu do charakteryzacji materiału na przykład w zakresie parametrów mikrostruktury, tzn. do defektów sieciowych typu rozkładów i gęstości dyslokacji, wtrąceń, mikropustek, aby opisać wzmocnienie i/lub osłabienie materiałów, głównie stopów metali, ale również do mierzenia przyłożonych i resztkowych naprężeń (Dobmann *et al.*, 1989).

Manuscript received December 13, 2005; accepted for print March 15, 2006